Structure of the triplet excited state of bromanil from time-resolved resonance Raman spectra and simulation

Mrinalini Puranik[a] and Siva Umapathy[b]
Department of Inorganic and Physical Chemistry, Indian Institute of Science, Bangalore-560012, India

Jaap G. Snijders
Theoretical Chemistry, Materials Science Centre, Rijksuniversiteit Groningen, Nijenborgh 4, 9747 AG Groningen, The Netherlands

Jayaraman Chandrasekhar
Department of Organic Chemistry, Indian Institute of Science, Bangalore-560012, India

Time-resolved resonance Raman (TR3) spectroscopy has been used to study the structure of the triplet excited state of bromanil. These experimental results were then simulated using parameters from density functional theoretical (DFT) calculations and wave packet dynamics, in order to understand the structure and mode-specific displacements of the resonant excited state. The transition dipole moments and the energy separation of the T_1 and T_n states were obtained from time-dependent DFT calculations. We have demonstrated application of the technique to tetrabromo-*p*-benzoquinone. From our calculations, the observed $T_1 \rightarrow T_n$ absorption spectrum has been assigned to the $^3B_g \rightarrow {}^3B_u$ transition. The geometry has been optimized for the resonant higher triplet state, T_n, and is found to be in good agreement with the predictions of the wave packet dynamical simulations. Mode-specific displacements of the triplet state geometry have been obtained from simulations and these have been rationalized with respect to the molecular orbital involved. Thus, we have demonstrated that from the simulations of the experimental TR3 spectral data, valuable additional information can be derived on the structure of the transient states that may then be used for elucidation of structure-reactivity correlation in the future.

I. INTRODUCTION

Time-resolved resonance Raman spectroscopy is a sensitive technique that has been demonstrated to be useful in addressing a wide range of chemical problems due to its electronic state and chromophoric selectivity.[1–4] It has been used to study electron transfer, transient intermediate kinetics and structure-reactivity relationships to name a few. While the experimental methodologies have progressed considerably in terms of both the varying time scales and the types of phenomenon addressed, the theoretical support has been generally directed towards the calculation of vibrational frequencies using quantum chemical methods. These are then used to obtain a better understanding of the structure and to support assignments of observed bands. However, little interpretation of the observed intensities in the excited state is made. This paper attempts to address the lacuna in utilizing the information contained in the intensities. In the ground state resonance Raman (RR) studies, the frequencies of the observed bands have been used to derive information on the structure, whereas the intensities have been utilized to understand the mode specific dynamics on the resonant excited state potential energy surface (PES), particularly near the Franck-Condon region.[5–13]

Generally, the time-dependent theory of resonance Raman intensities, originally put forth by Lee and Heller[5] has been applied with much success. The dynamics of a wide range of fast chemical processes involving, e.g., bacteriorhodopsin,[6] stilbene,[7,8] azodyes,[9–11] chlorine dioxide,[12] *N*-methylacetamide,[13] etc., has been probed. Application of the time-dependent theory of resonance Raman intensities to molecules in their ground state has been reviewed extensively.[6,14–18] Two approaches are generally used: (i) The molecular parameters may come from a purely empirical model, and these are then optimized iteratively to obtain the best fit to the observed spectra,[6–12,14–18] or (ii) molecular parameters are obtained from *ab initio* calculations and the Raman intensities are predicted and compared with experiment.[13,19–21] The former method allows a direct interpretation of the observed intensities and the latter is more likely to be used to judge the reliability of various computational methods. Our group has applied the former method to trans-azobenzene[9,10] in order to understand the dynamics of isomerization. The technique was also developed further to obtain the vibrational and solvent reorganization energies from the total reorganization energy.[11] The success of these wave packet dynamical methods in the ground state molecules spurred attempts to apply the theory for

[a]Also at: Department of Organic Chemistry, Indian Institute of Science, Bangalore-560012, India.
[b]Author to whom correspondence should be addressed.
Phone: +91-(0)80-3601234, Fax: +91-(0)80-3601552.
Electronic mail:umapathy@ipc.iisc.ernet.in

short-lived transient intermediates like radical cations[19,20] and triplet excited states[21] that are experimentally observed using time-resolved resonance Raman spectroscopy. These developments are important for most organic photochemical processes, including in quinones, in which the photoreactive state is the lowest triplet state. Thus the knowledge of the mode-specific dynamics of the triplet excited state is essential to understand the reactivity. It is also important to know the nature of the potential energy surface of the higher triplet state in the Franck-Condon region. While some information on the structure of the lowest triplet state (T_1) is obtained from the time-resolved resonance Raman spectra as well as *ab initio* and DFT calculations, it is more difficult to determine properties of the potential energy surfaces of higher triplet states.

Previous attempts by Wilbrandt and co-workers[21] to predict triplet excited-state Raman spectra involved an *ab initio* calculation of the optimized geometry of the transient state (e.g., T_1). This was followed by a CI calculation to obtain the transition dipole moment of the $T_1 \rightarrow T_n$ transition, where T_n denotes the resonant triplet state. Displacements in equilibrium geometries between the T_1 and T_n states were computed. These were used to predict Raman spectra, which were compared with the experimentally observed spectra. Similar procedures were followed for radical cations as well.[19,21] This approach gave a satisfactory agreement between the calculated and experimentally determined resonance Raman spectra. However, for larger polyatomics, CI calculations rapidly become computationally intractable. It is also desirable that the experimentally measured intensities should be used to extract information on the PES in a more direct way rather than by comparison of predicted and observed spectra alone.

Recently, several studies have demonstrated the success of density functional theoretical techniques in the prediction of vibrational frequencies.[22–28] Accurate normal mode descriptions are a prerequisite for the inference of excited-state geometry changes from computed potential energy displacements. The development of time-dependent density functional theory (TDDFT) has provided a means for the economical computation of transition dipole moments at a given geometry.[29,30] It is desirable therefore, to apply these methods in the determination of the excited-state properties. Thus, in this paper, we have combined the technique of wave packet propagation with molecular parameters and energies from density functional theory (DFT) and time-resolved resonance Raman experiments to simulate the triplet excited state spectra of bromanil. To our knowledge, this is the first attempt to model the intensities of the triplet excited state using a combination of experimentally and theoretically determined parameters.

The parent benzoquinone and its fluorinated and chlorinated analogues have been studied extensively for their applications in biology and chemistry as electron acceptors in photochemical reactions. Benzoquinone is a well-studied system, both theoretically[24,31] and experimentally.[32] We have been involved in systematically investigating the effects of various substitutions on the structure of benzoquinone in the excited state.[24,26–28,33–36] In fluoranil,[34] we have shown that the structure of the triplet excited state is less delocalized than in triplet benzoquinone due to the presence of perfluoro effect. Two opposite effects play a role in determining properties of perhalo substituted benzoquinones: inductively σ-withdrawing nature and the π-donation of the lone pairs of halogens.[37] Subtle changes in the structure due to substitution are known to alter the reactivity considerably in ketones. In bromanil, it is expected that the molecular properties would differ considerably from fluoranil, although both are halogen substitutions, since bromine is larger in size and less electron withdrawing than fluorine. Thus, we have taken the bromanil triplet excited state as an example to understand the mode-dependent shifts in the triplet state potential energy surfaces predicted by the simulation of the resonance Raman intensities.

II. EXPERIMENTAL METHODS

Experimental methods and procedures used for the TR3 spectroscopy have been described previously.[35] Briefly, the pump beam is the third harmonic output of a 1064 nm fundamental from a Nd:YAG laser (DCR 11, Spectra Physics). The probe beam is obtained from an optical parametric oscillator (OPO) which is pumped by the third harmonic of 1064 nm output from an Nd:YAG laser (GCR 250, Spectra Physics). The probe wavelength 512 nm was obtained from the OPO. The pulses had typical energies of 2.5 mJ and were *ca.* 10 ns in temporal width for both pump and probe lasers. The scattered light was dispersed using a SPEX double monochromator with two 600 groves/mm gratings. The multichannel detector used was a liquid Nitrogen cooled CCD from Princeton Instruments with 576×378 pixels. The spectra have been calibrated using known solvent bands as reference, and the spectral resolution has been estimated as 5 cm^{-1}. The concentration used for the Raman experiments was *ca.* 2 mM.

Bromanil used was purchased from Aldrich Chemicals. Both, bromanil and the solvents were of analytical grade and used without further purification. Sample solutions were circulated through a capillary at a rate of about 10 ml per minute to avoid possible accumulation of photoproducts. The probe only spectra were recorded periodically to confirm the absence of photoproducts.

III. THEORY AND COMPUTATIONAL METHODS

Density functional theoretical calculations were performed with the Amsterdam Density Functional (ADF99) package[38] on a cluster of IBM RS 6000/43P workstations. Calculations for the triplet excited state used the unrestricted formalism. The basis set used was TZP (Basis IV in ADF terminology) that is a part of the ADF program.[38] The singlet-triplet excitation energies and the transition dipole lengths were computed using TDDFT as implemented in the Response[29] code in the ADF package of programs. Density functional calculations involved the local density approximation of Vosko, Wilk and Nussair (VWN),[39] gradient-corrected exchange functional proposed by Becke[40] and the correlation functional of Lee, Yang and Parr.[41] Normal mode analysis was carried out using NMODES,[24] a program devel-

oped in our laboratory which used the normal mode eigen vectors computed using the ADF package to compute the potential energy distribution. Wave packet dynamical simulations were carried out using MATLAB on an IBM RS 6000 workstation, using the analytical solutions mentioned below. The Fourier transform and inverse Fourier transform routines used were a part of the MATLAB library. Time step used for the simulation was 0.01 fs.

Lee and Heller's[5] time-dependent approach to resonance Raman scattering has been used to simulate the observed absorption and the relative Raman intensities. This time-domain picture of RR scattering has an intuitive appeal due to the simple physical picture that it provides for an understanding of the RR process. In this approach, the energy denominator of the sum-over-states expression of the Raman polarizability in Eq. (1)

$$\alpha_{if}(E_L)=M^2\sum_{\nu}\frac{\langle f|\nu\rangle\langle\nu|i\rangle}{\varepsilon_\nu-\varepsilon_i+E_0-E_L-i\Gamma} \tag{1}$$

is written in the form of an integral over a time variable.[5] If all the PES's are assumed to be harmonic and separable, we obtain the following expression for the Raman cross section in the time-domain,[5,42]

$$\sigma_{i\to f}(E_L)=\frac{8\pi E_s^3E_Le^4M^4}{9\hbar^6c^4}\left|\int_0^\infty\langle f|i(t)\rangle \times\exp\left[i(E_L+E_i)t/\hbar-\frac{\Gamma t}{\hbar}-\frac{\theta^2t^2}{2\hbar}\right]dt\right|^2, \tag{2}$$

and the corresponding expression for the absorption spectrum is given by,

$$\sigma_A(E_L)=\frac{4\pi e^2M^2E_L}{6\hbar^2c}\int_{-\infty}^{\infty}\langle i|i(t)\rangle\exp\left[i(E_L+E_i)t/\hbar-\frac{\Gamma|t|}{\hbar}-\frac{\theta^2t^2}{2\hbar}\right]dt. \tag{3}$$

Here, $|i(t)\rangle$ denotes the wave packet evolving on the resonant excited-state surface (RES) at various intervals of time (t), under the influence of excited state vibrational Hamiltonian, $H_{\rm ex}$ given by the following expression:

$$|i(t)\rangle=\exp\left(-\frac{iH_{\rm ex}t}{\hbar}\right)|i\rangle, \tag{4}$$

where $\exp(-iH_{\rm ex}t/\hbar)$ is the time evolution operator. Further, we have also assumed that there is no change in the vibrational normal modes on excitation, i.e., Duschinski rotation is not taken into account. The incident and scattered photon energies are E_L and E_8; E_i is the zero-point vibrational energy of the T_1 state, and M is the electronic transition dipole length evaluated at the equilibrium geometry of the T_1 state for the transition from the T_1 state to the resonant excited state (RES, T_n), e is the electronic charge and c is the velocity of light. Motion of the time-evolving wave packet on the excited state is damped by two terms, $\exp(-\Gamma t/\hbar)$ and $\exp(-\theta^2t^2/2\hbar)$, which include broadening due to finite life-time (Γ) as well as that induced by solvent (θ).

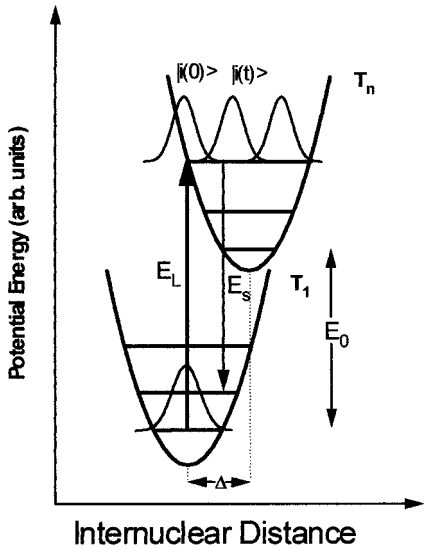

FIG. 1. Schematic representation of the physical picture provided by the time-dependent theory of resonance Raman intensities.

The physical interpretation provided by these equations is that the system is initially in a state $|i\rangle$, a vibrational eigen state of the lower triplet state (T_1) surface. As shown in Fig. 1, the wave packet is transported to the T_n state via interaction of the transition dipole moment eM, of the $T_1\to T_n$ transition with the incident radiation of energy E_L. The vibrational state $|i\rangle$ is not a stationary state of the T_n state and starts evolving under the influence of the excited state Hamiltonian, $H_{\rm ex}$ and is denoted by $|i(t)\rangle$. The absorption and Raman cross sections are obtained by taking the overlap of this time-evolving wave function with the ground vibrational state of the T_1 state, $|0\rangle$ (for absorption) and the first excited vibrational state of T_1 $|1\rangle$ (for Raman).

The approximations stated earlier of harmonicity, separability, and equal frequencies lead to simplified expressions for the absorption and Raman cross sections[15] given by,

$$\sigma_A(E_L)=\frac{4\pi e^2M^2}{6\hbar^2c}\int_{-\infty}^{\infty}\exp\left[i(E_L-E_0)t/\hbar-\Gamma|t|/\hbar-\frac{\theta^2t^2}{2\hbar}\right]\prod_{j=1}^{N}\exp\left\{-\frac{\Delta_j^2}{2}[1-\exp(-i\omega_jt)]\right\}dt, \tag{5}$$

and

$$\sigma_{0\to1}(E_L)=\frac{8\pi e^4M^4E_S^3E_L}{9\hbar^6c^4}\left|\int_0^\infty\exp\left[i(E_L-E_0)t/\hbar-\Gamma|t|/\hbar-\frac{\theta^2t^2}{2\hbar}\right]\frac{\Delta_1}{\sqrt{2}}(e^{-i\omega_1t}-1)\times\prod_{j=1}^{N}\exp\left\{-\frac{\Delta_j^2}{2}[1-\exp(-i\omega_jt)]\right\}dt\right|^2, \tag{6}$$

where, E_0 is the separation between the zero-point energies of the T_1 and T_n states and Δ_j denotes the relative dimensionless displacements between the PES's of the T_1 and T_n

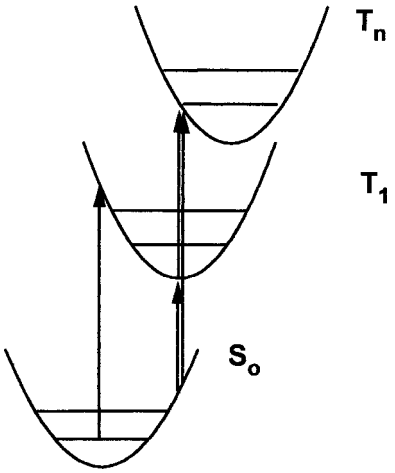

FIG. 2. Schematic representation of the energy differences in the singlet and triplet manifolds computed using TDDFT and DFT methods.

states along the jth mode. Therefore the parameters required for the simulation of the resonance Raman spectrum are the zero-zero energy (E_0), the transition dipole length for the $T_1 \rightarrow T_n$ transition, guess values for the displacements (Δ_j) and vibrational frequencies (ω_j) of the observed normal modes. In the following, we discuss each of these parameters along with the procedures used to obtain initial guesses in detail.

Initially, a DFT calculation was carried out to obtain the optimized geometry of the ground state (S_0) of bromanil. Vibrational frequencies were computed and it was confirmed that the geometry is a minimum. Singlet-singlet and singlet-triplet excitations of bromanil were computed at this geometry using TDDFT. A comparison of the computed and experimentally reported S_0-T_1 gap was made to identify the lowest triplet excited state. The geometry was optimized for the T_1 state and vibrational frequencies were computed.

Subsequently, excitation energies are computed at the optimized triplet state geometry in order to identify the resonant triplet state by comparison with the observed maximum in the $T_1 \rightarrow T_n$ transient absorption spectrum and predicted excitation energies illustrated schematically in Fig. 2. This is defined as the difference in energies:

$$\Delta E(T_1 \rightarrow T_n) = E(S_{\text{trip geom}} \rightarrow T_1) - E(S_{\text{trip geom}} \rightarrow T_n). \tag{7}$$

In principle, the transition dipole moment is a function of the nuclear coordinates, Q, because the Born-Oppenheimer electronic states depend parametrically on the nuclear coordinates. This coordinate dependence is neglected when on resonance with a strongly allowed transition (Condon approximation), i.e., $M(Q)$ is replaced with $M(Q_0)$, where Q_0 is the fixed T_1 state geometry. The transition dipole moment for the $T_1 \rightarrow T_n$ transition therefore is computed at the equilibrium geometry of the T_1 state.

In general, TDDFT only provides the transition dipole moment between the ground and excited states. Hence, the computation of the transition dipole moment between two excited (triplet) states used here requires some explanation. However, the formalism of TDDFT is very similar to the singly excited CI calculation. If we assume that the Kohn-Sham single determinant is a reasonable, approximate description of the excited states in terms of a linear combination of determinants, singly excited with respect to the ground state. If we make this approximation, the transition dipole moments between these excited states are easily calculated.[43]

The separation of the T_1 and the T_n states, E_0, determines the position of the absorption band. An initial guess is obtained from the computed excitation energy using TDDFT. The energy computed from the TDDFT calculation corresponds to the Franck-Condon excitation energy. The zero-zero separation is expected to be smaller than this value, in principle equal to the ΔSCF energy, i.e., difference in the minimized energies of the T_1 and T_n states. The guess displacements for the simulation are calculated from the ratios of relative intensities of the observed Raman spectra using the approximation $I_j \propto \Delta_j^2 \omega_j^2$.[44]

Finally, the broadening parameters affect the shape of the absorption spectrum but do not change the integrated absorption intensity. Fitting of the absorption spectrum alone, without the simultaneous modeling of the Raman excitation profile, can determine the total line width. However, relative magnitudes of homogeneous (Γ) and inhomogeneous (Θ) broadening values computed from these simulations cannot be considered unique since the absorption spectrum is not sensitive to the partitioning of the homogeneous and inhomogeneous components.[15,16]

IV. RESULTS AND DISCUSSION

In a previous paper, we have reported the time-resolved resonance Raman spectra and assignments of the triplet excited state of bromanil in carbon tetrachloride.[28] The triplet state was populated via the singlet excited state by intersystem crossing by exciting with a pump laser at 355 nm. The probe laser at 512 nm, close to the maximum of the triplet-triplet absorption band (515 nm) was used to obtain the Raman spectrum. Four bands were observed at 1561, 1396, 1178, and 961 cm^{-1} in the Raman spectrum shown in Fig. 3. The bands at 1561, 1396, and 961 cm^{-1}, were assigned to fundamentals of a_g symmetry.[28] The assignments, computed spectra and potential energy distribution for the observed totally symmetric modes are summarized in Table I. The band at 1178 cm^{-1} was assigned[28] to either a fundamental or overtone of a nontotally symmetric mode due to vibronic coupling of this mode with the nearby excited state, $^3B_{1g}$.

Since the objective of this paper is to compute the resonance Raman intensities and therefore the mode-dependent displacements of the PES of the excited state, we have modeled only these totally symmetric modes in the following intensity analyses. The measured depolarization ratios of all the totally symmetric bands are close to 0.3,[28] an indication that the intensities are derived from a single resonant state. It has been shown earlier by Tannor and Heller[42] that the wave packet dynamics in the harmonic case is separable into subspaces comprised of normal modes belonging to the same irreducible representation. The motion of the center of the wave packet is restricted to the totally symmetric subspace.

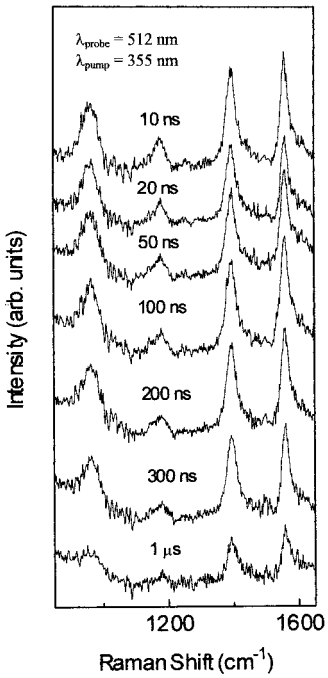

FIG. 3. Time-resolved resonance Raman spectra of triplet bromanil in carbon tetrachloride at various time delays between the pump and probe.

Only the totally symmetric bands are expected to be enhanced in a resonance Raman experiment and to have displacements in the excited state. The effect of the nontotally symmetric modes is only to broaden the spectrum.[42]

The optimized geometries and vibrational frequencies of the ground and triplet excited state of bromanil have been discussed in detail elsewhere.[28] Briefly, the triplet state was found to be of a lower symmetry (C_{2h}) than the ground state (D_{2h}). The effect of electronic excitation to the triplet state was found to be the largest along the C═O bond followed by the C═C bond. The C–C bond lengths were shortened on excitation. Both the high frequency modes at 1561 and 1395 cm^{-1} were predicted to be coupled modes with different relative contributions of C═O and C═C stretching.

Table II lists the predicted singlet-triplet excitations computed at the optimized ground state geometry by TDDFT. The lowest S_0-T_n gap corresponds to the $b_{1g}\rightarrow b_{2g}$ transition of 1.62 eV energy leading to a triplet state of B_{3g} symmetry. This is a π-π^* transition from the HOMO of b_{1g} symmetry of the ground state to the LUMO of b_{2g} symmetry. We note that there is another singlet-triplet excitation close to this from the HOMO-1 orbital of b_{3g} symmetry to the LUMO with excitation energy 1.74 eV of n-π^* character. Hence, TDDFT calculations predict relative ordering of the

TABLE I. Computed and experimental frequencies and potential energy distributions of the normal modes of triplet excited state of bromanil.

Sym.	PED%	Experimental	Calculated
a_g			
	C═C(35), C–C(27), C═O(20)	1561	1525
	C═O(60), C═C(37)	1395	1311
	C–Br(54), C–C(36)	965	901

TABLE II. Singlet-triplet excitation energies computed at the optimized ground state geometry (D_{2h}) of bromanil by TDDFT calculations.

	State	Major MO's involved	Energy (eV)
1.	$^3B_{1g}$	$4b_{3g}\rightarrow 5b_{2g}$	1.62
2.	$^3B_{3g}$	$8b_{1g}\rightarrow 5b_{2g}$	1.74
3.	$^3B_{3u}$	$5b_{1u}\rightarrow 5b_{2g}$	2.13
4.	^3A_u	$9b_{2u}\rightarrow 5b_{2g}$	2.23
5.	$^3B_{1u}$	$9b_{3u}\rightarrow 5b_{2g}$	2.35
6.	$^3B_{3g}$	$7b_{1g}\rightarrow 5b_{2g}$	2.53
7.	^3A_u	$8b_{2u}\rightarrow 5b_{2g}$	2.90
8.	^3A_g	$4b_{2g}\rightarrow 5b_{2g}$	2.96
9.	$^3B_{2g}$	$10a_g\rightarrow 5b_{2g}$	3.12
10.	$^3B_{2u}$	$3a_u\rightarrow 5b_{2g}$	3.14

π-π^* and n-π^* states in agreement with the experimental data of Schleglova and co-workers[37] where they have reported that the lowest triplet state in bromanil is the π-π^* state from their luminescence experiments.

Table III lists the singlet-triplet excitations computed at the triplet state geometry. As expected, the S_0-T_1 gap is reduced to 1.20 eV and corresponds to the transition $12b_g \rightarrow 15a_g$ in C_{2h} symmetry. The experimental absorption spectrum shown in Fig. 3 has a maximum at 2.41 eV. Therefore, the resonant excited state is expected at a singlet-triplet gap of 3.61 eV (1.20 eV + 2.41 eV). The transition with the energy closest to the maximum of the observed absorption spectrum (within the symmetry-allowed transitions) is identified as the $12b_g\rightarrow 13a_u$ (81%) corresponding to the state, ^3B_u with excitation energy 3.74 eV. The occupations of the unpaired electrons of the RES are: $12b_g(1)13a_u(1)$, leading to a final triplet state of B_u symmetry. Hence, the observed absorption spectrum is a transition from $^3B_g\rightarrow{}^3B_u$, where the unpaired electron from the $15a_g$ orbital is excited to the $13a_u$ orbital. The transition dipole length computed from TDDFT is $\langle 15a_g|\vec{\mu}|13a_u\rangle = 0.97$ Å. This computed value has been kept constant during the simulation. The T_1-T_n energy predicted by TDDFT, 2.51 eV (20 245 cm^{-1}) was used as the initial value of E_0.

Figure 4 shows the final simulated absorption spectrum (solid line) and Fig. 5 shows the excitation profiles for the three modes. The best-fit parameters obtained are $E_0 = 16\,915\ cm^{-1}$, $M = 0.97$ Å, $\Gamma = 450\ cm^{-1}$ and Θ

TABLE III. Singlet-triplet excitation energies computed at the optimized triplet excited state geometry (C_{2h}) using TDDFT calculations.

	State	Major MO's involved	Energy (eV)
1.	^3B_g	$12b_g\rightarrow 15a_g$	1.20
2.	^3A_u	$12a_u\rightarrow 15a_g$	1.70
3.	^3B_u	$14b_u\rightarrow 15a_g$	1.78
4.	^3B_u	$13b_u\rightarrow 15a_g$	1.98
5.	^3A_u	$11a_u\rightarrow 15a_g$	2.56
6.	^3A_u	$10a_u\rightarrow 15a_g$	2.80
7.	^3B_u	$12b_u\rightarrow 15a_g$	3.22
8.	^3B_u	$12b_g\rightarrow 13a_u$ (81%) $11b_g\rightarrow 13a_u$ (16%)	3.74
9.	^3A_u	$12a_u\rightarrow 16a_g$	4.45

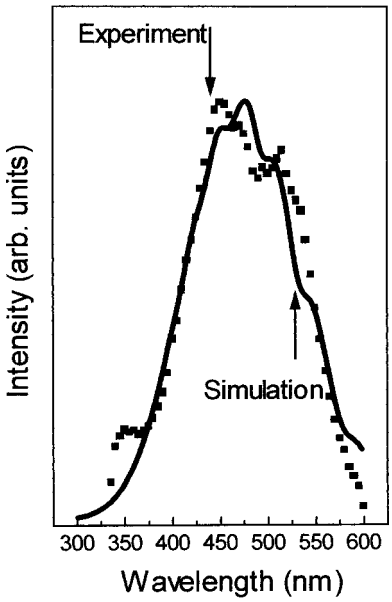

FIG. 4. Experimental (squares) and simulated (solid line) absorption spectra of triplet bromanil in carbon tetrachloride.

$=150\,\mathrm{cm}^{-1}$. The corresponding mode-specific dimensionless displacements have been given in Table IV and the simulated spectrum has been shown in Fig. 6. The PES displacements obtained are similar for all three modes with 1.51 for the highest frequency mode at 1561 cm^{-1}, 1.61 and 1.53 for the modes at 1396 cm^{-1} and 965 cm^{-1}, respectively. As shown in Fig. 7, the mode at 1561 cm^{-1} has contributions from the C═C str. C═O str. and the C–C str. Similarly for the mode at 1396 cm^{-1}, both the C═O and C═C str. are involved. We note that the sign of the displacement is not determined by

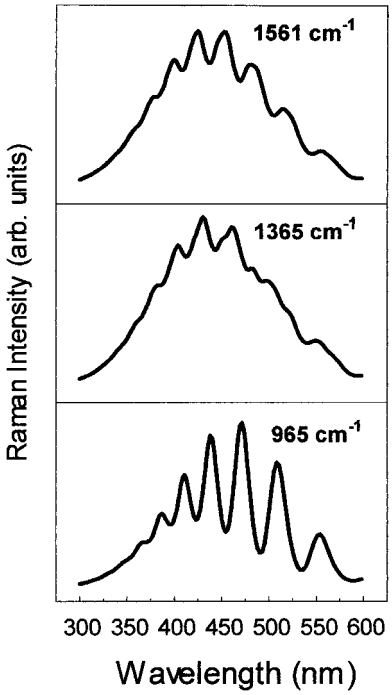

FIG. 5. Simulated Raman excitation profiles for each of the observed fundamental modes.

TABLE IV. Best-fit values of the dimensionless displacements obtained from the simulation with $E_0 = 16\,915\,\mathrm{cm}^{-1}$, $\Gamma = 450\,\mathrm{cm}^{-1}$, $\Theta = 150\,\mathrm{cm}^{-1}$.

Frequency ($\omega_i\,\mathrm{cm}^{-1}$)	Displacement (Δ_i)	Relative intensities	
		Experimental	Calculated
1561	1.51	1.0	1.0
1396	1.61	0.87	0.88
965	1.53	0.58	0.56

these simulations, since only the square of the displacement appears in the analytical expressions of the cross sections. Therefore, interpretation of the computed displacements, in terms of the changes in bond lengths, has been carried out by using the knowledge of the nature of the ground state MO involved in the formation of the T_n state.

The similar displacements in all the modes indicate that the changes in structure in RES with respect to the T_1 state are not localized to a specific part of the molecule but are spread over the entire molecule. This may be rationalized from the nature of the ground state molecular orbitals involved in these states as follows. The T_1 state involves population of the LUMO, which is delocalized over the carbonyl groups and the C–C bonds. It was shown earlier[28] that the geometry of the T_1 state could be explained from the nodal structure of the LUMO of the ground state. The LUMO has bonding interaction with the C–C–C atoms and antibonding interaction between the carbon and oxygen of the carbonyl group. As a consequence, in the T_1 state, the C–C bonds were shortened and the C═O bonds were lengthened in comparison with the ground state. The T_n state is formed by removing the electron from the LUMO and populating the higher unoccupied MO($13a_u$) which is shown in Fig. 8. The orbital has antibonding character between the carbon atoms of the C═C bond. Therefore, qualitatively, the expected

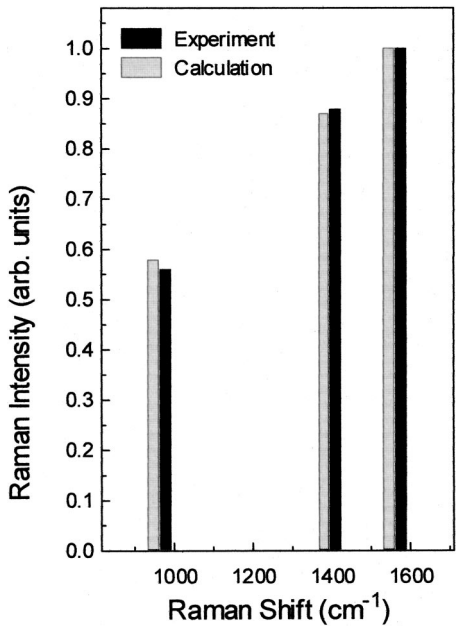

FIG. 6. Experimental and simulated resonance Raman intensities of bromanil.

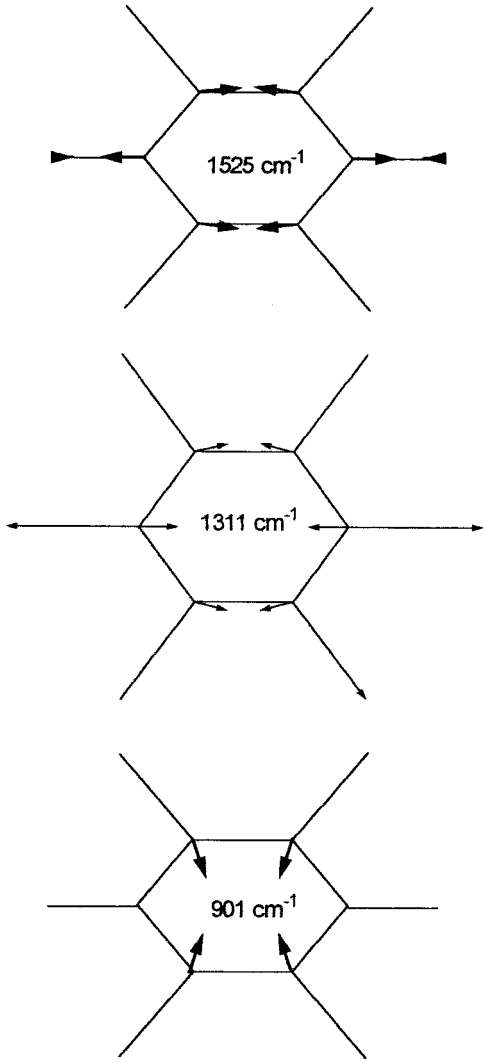

FIG. 7. Normal mode displacements of triplet bromanil for the observed modes.

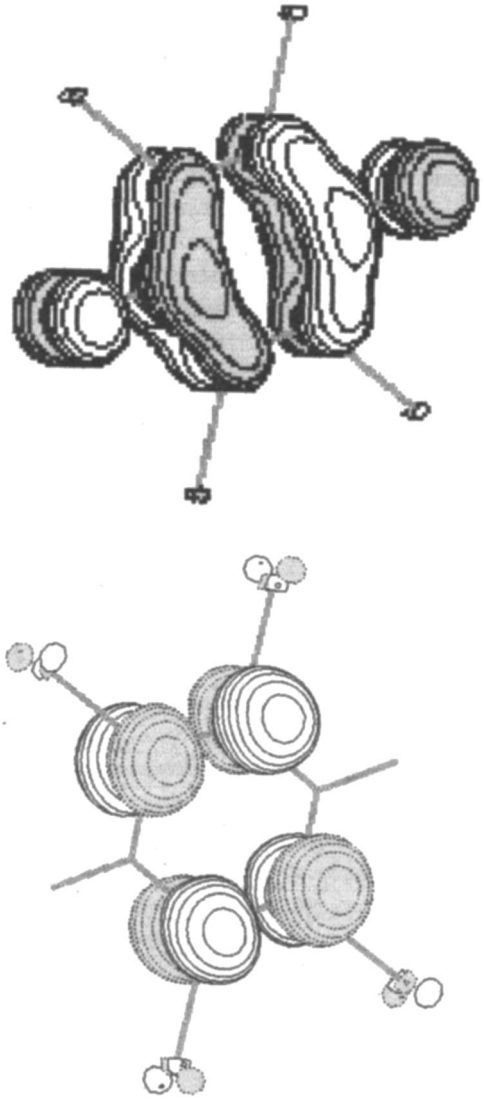

FIG. 8. Computed molecular orbitals of bromanil in the ground state LUMO and the $13a_u$ orbital.

changes in the geometry of bromanil in the T_n state as compared to the T_1 state are: (1) The C═O bond length should decrease due to removal of the electron from the C═O antibonding LUMO, (2) the C–C bond length should increase, and (3) the C═C bond should be longer due to antibonding nature of the a_u orbital. The computed displacements bear out the expected geometrical changes.

Table V lists the optimized geometry in the T_n state identified from comparison of the experimental absorption and TDDFT calculations. Previously reported geometries of the ground state and T_1 state are also given for comparison. In the T_n state, the C═C and C–C bond lengths are increased to 1.389 Å and 1.480 Å. The C═O bond length decreases to 1.215 Å. The trends in the geometries predicted using DFT are in agreement with those predicted by the simulated displacements. The difference in the bonding energies (ΔE_{SCF}) of the T_1 and the T_n states is found to be 16 739 cm^{-1}. The best-fit value of E_0 obtained from the simulations was 16 915 cm^{-1}, close to the SCF energy difference. The difference between the computed Franck-Condon excitation energy (TDDFT) and zero-zero separation (ΔE_{SCF}) and that obtained from experiments ($\lambda_{\max}$) and simulations (E_0) are close to each other.

V. SUMMARY

The theory of resonance Raman intensities has been applied to the triplet excited state using the techniques of wave packet dynamics and density functional theory. The simula-

TABLE V. Calculated geometries of the ground and lowest triplet excited states and the resonant triplet state of bromanil.

	Ground state (D_{2h})	Lowest triplet state $T_1(C_{2h})$	Excited triplet state $T_n(C_{2h})$
$R_{(C=C)}$	1.341	1.369	1.389
$R_{(C=O)}$	1.212	1.251	1.215
$R_{(C-C)}$	1.485	1.440	1.480
$R_{(C-Br)}$	1.883	1.885	1.889
$\alpha_{(C=C-C)}$	121.6	122.2	121.5
$\alpha_{(C-C-C)}$	116.9	115.6	116.7
$\alpha_{(C=C-Br)}$	123.5	122.8	122.3

tions yield valuable information on the structure and PES of the resonant higher triplet state. The observed $T_1 \rightarrow T_n$ absorption spectrum is assigned to the ${}^3B_g \rightarrow {}^3B_u$ transition. The geometry has been optimized for the resonant higher triplet state, T_n, and is found to be in good agreement with the predictions of the wave packet dynamical simulations. The triplet-triplet energy separation predicted by TDDFT is close to the separation obtained from the λ_{max} of the transient absorption experiment (Franck-Condon excitation energy) and the zero-zero energy separation obtained from DFT (ΔSCF) is close to the best-fit value obtained from the simulations.

Thus, it has been demonstrated that TR3 spectra can be simulated to obtain valuable structural and dynamical information like the energy separation between the lowest triplet state and the resonant excited-state (T_n), nature of the T_n and its PES and initial mode-specific dynamics of the reactive triplet state. However, it is important to appreciate the caveats in such an approach. It is well known that accurate measurement of resonance Raman intensities is difficult. While the transient state excitation profiles would in principle yield more information, they are prone to several possible sources of error, which must be carefully accounted for. The simple analytical solutions used here assume only one resonant excited state. Therefore, these cannot be applied to molecules where the transient state resonance Raman spectra indicate the presence of multiple electronic states.

The dimensionless displacement parameters obtained from these simulations are relative values and the sign of the displacement is not known. Combined information from simulations and DFT enables interpretation of the computed displacements to physically meaningful changes in geometry. Thus, it is possible to extract valuable information on the mode-specific dynamics in the triplet excited state, which is a precursor to several photochemical reactions.

ACKNOWLEDGMENTS

The authors thank the Department of Science and Technology (DST) and the Council of Scientific and Industrial Research (CSIR), Government of India, for financial support. One of the authors (M.P.) thanks Unilever India Inc., NUFFIC, and Dutch Ministry for Culture, Education and Science, The Netherlands, for a visiting fellowship.

[1] R. E. Hester, in *Advances in Infrared and Raman Spectroscopy*, edited by R. J. H. Clark and R. E. Hester (Heyden, London, 1978), Vol. 4, p. 1.
[2] G. H. Atkinson, in *Advances in Infrared and Raman Spectroscopy*, edited by R. J. H. Clark and R. E. Hester (Heyden, London, 1982), Vol. 9, p. 1.
[3] H. Hamaguchi, in *Vibrational Spectra and Structure*, edited by J. R. Durig (Elsevier, Amsterdam, 1987), Vol. 16, p. 227.
[4] G. N. R. Tripathi, in *Time Resolved Spectroscopy*, edited by R. J. H. Clark and R. E. Hester (John Wiley and Sons, Ltd., London, 1989), Vol. 18, Chapter 4, p. 157.
[5] S. Lee and E. J. Heller, J. Chem. Phys. **71**, 4777 (1979).
[6] R. Mathies, in *Chemical and Biochemical Applications of Lasers*, edited by C. B. Moore (Academic, New York, 1979), Vol. 4, p. 55.
[7] A. B. Myers and R. A. Mathies, J. Chem. Phys. **81**, 1552 (1984).
[8] J. Rodier and A. B. Myers, J. Am. Chem. Soc. **115**, 10791 (1993).
[9] N. Biswas and S. Umapathy, J. Chem. Phys. **107**, 7849 (1997).
[10] N. Biswas and S. Umapathy, Chem. Phys. Lett. **236**, 24 (1995).
[11] N. Biswas and S. Umapathy, Chem. Phys. Lett. **294**, 181 (1998).
[12] A. P. Esposito, C. E. Foster, R. A. Beckman, and P. J. Reid, J. Phys. Chem. A **101**, 5309 (1997).
[13] L. M. Markham and B. S. Hudson, J. Phys. Chem. **100**, 2731 (1996).
[14] E. J. Heller, Acc. Chem. Res. **14**, 368 (1981).
[15] A. B. Myers and R. A. Mathies, in *Biochemical Applications of Raman Spectroscopy*, edited by T. G. Spiro (Wiley, New York, 1987), Vol. 2, p. 1.
[16] A. B. Myers, J. Raman Spectrosc. **28**, 389 (1997); A. B. Myers, Chem. Rev. **96**, 911 (1996); A. B. Myers, in *Laser Techniques in Chemistry*, Techniques of Chemistry Series, Vol. 23, edited by A. B. Myers and T. R. Rizzo (Wiley and Sons Inc., New York, 1995), pp. 325–384.
[17] J. L. Zink and K.-S. K. Shin, Adv. Photochem. **16**, 119 (1991).
[18] N. Biswas and S. Umapathy, Curr. Sci. **74**, 328 (1998).
[19] L. M. Markham, L. C. Mayne, B. S. Hudson, and M. Z. Zgierski, J. Phys. Chem. **97**, 10319 (1993); B. S. Hudson and L. M. Markham, J. Raman Spectrosc. **29**, 489 (1998).
[20] T. Keszthelyi, G. Balakrishnan, R. Wilbrandt, W. A. Yee and F. Negri, J. Phys. Chem. A **104**, 9121 (2000); A. M. Brouwer, J. M. Zwier, C. Svendsen, O. S. Mortensen, F. W. Langkilde, and R. Wilbrandt, J. Am. Chem. Soc. **120**, 3748 (1998); A. M. Brouwer, C. Svendsen, O. S. Mortensen, and R. Wilbrandt, J. Raman Spectrosc. **29**, 439 (1998).
[21] F. W. Langkilde, R. Wilbrandt, A. M. Brouwer, F. Negri, and G. Orlandi, J. Phys. Chem. **98**, 2254 (1994); F. W. Langkilde, R. Wilbrandt, S. Moller, A. M. Brouwer, F. Negri, and G. Orlandi, J. Phys. Chem. **95**, 6884 (1991); F. Negri, G. Orlandi, A. M. Brouwer, F. W. Langkilde, S. Moller, and R. Wilbrandt, J. Phys. Chem. **95**, 6895 (1991); F. Negri, G. Orlandi, A. M. Brouwer, F. W. Langkilde, and R. Wilbrandt, J. Chem. Phys. **90**, 5944 (1989).
[22] S. E. Boesch and R. A. Wheeler, J. Phys. Chem. **99**, 8125 (1995); S. E. Boesch and R. A. Wheeler, J. Phys. Chem. **101**, 8351 (1997).
[23] D. Pan, L. C. T. Shoute, and D. L. Phillips, J. Phys. Chem. A **103**, 6851 (1999); D. Pan, L. C. T. Shoute, and D. L. Phillips, J. Phys. Chem. A **104**, 4140 (2000).
[24] P. Mohandas and S. Umapathy, J. Phys. Chem. A **101**, 4449 (1997).
[25] N. Biswas and S. Umapathy, J. Phys. Chem. **101**, 5555 (1997); N. Biswas and S. Umapathy, J. Phys. Chem. **104**, 2734 (2000).
[26] G. Balakrishnan, P. Mohandas, and S. Umapathy, Spectrochim. Acta, Part A **53**, 153 (1997).
[27] G. Balakrishnan, P. Mohandas, and S. Umapathy, J. Phys. Chem. A (in press).
[28] M. Puranik, J. Chandrasekhar, J. G. Snijders, and S. Umapathy, J. Phys. Chem. (unpublished).
[29] S. J. A. van Gisbergen, J. G. Snijders, and E. J. Baerends, Comput. Phys. Commun. **118**, 119 (1999).
[30] A. Rosa, E. J. Baerends, S. J. A. van Gisbergen, E. van Lenthe, and J. G. Snijders, J. Am. Chem. Soc. **121**, 10356 (1999); S. J. A. van Gisbergen, J. A. Groeneveld, A. Rosa, J. G. Snijders, and E. J. Baerends, J. Phys. Chem. A **103**, 6835 (1999); S. J. A. van Gisbergen, J. G. Snijders, and E. J. Baerends, Phys. Rev. Lett. **78**, 3097 (1997).
[31] D. M. Chipman and M. F. Prebenda, J. Phys. Chem. **90**, 5557 (1986).
[32] R. Rossetti and L. E. Brus, J. Am. Chem. Soc. **108**, 4718 (1986); S. M. Beck and L. E. Brus, J. Am. Chem. Soc. **104**, 4789 (1982); R. H. Schuler, G. N. R. Tripathi, M. F. Prebenda, and D. M. Chipman, J. Phys. Chem. **87**, 3101 (1983).
[33] G. Balakrishnan, A. Babaei, A. J. McQuillan, and S. Umapathy, J. Biomol. Struct. Dyn. **16**, 123 (1998); G. Balakrishnan and S. Umapathy, J. Mol. Struct. **475**, 5 (1999).
[34] G. Balakrishnan and S. Umapathy, Chem. Phys. Lett. **270**, 557 (1997); G. Balakrishnan and S. Umapathy, J. Chem. Soc., Faraday Trans. **93**, 4125 (1997); M. Puranik, H. Mohapatra, G. Balakrishnan, J. Chandrasekhar, and S. Umapathy, Asian J. Phys. **2**, 189 (1998).
[35] G. Balakrishnan, P. Mohandas, and S. Umapathy, J. Phys. Chem. **100**, 16472 (1996).
[36] M. Puranik, J. Chandrasekhar, and S. Umapathy, Chem. Phys. Lett. **337**, 224 (2001).
[37] N. A. Shcheglova, D. N. Shigorin, G. G. Yakobson, and L. Sh. Tushishvili, Russ. J. Phys. Chem. **43**, 1112 (1969).
[38] (a) ADF 1999, E. J. Baerends, A. Bérces, C. Bo *et al.*; (b) E. J. Baerends, D. E. Ellis, and P. Ros, Chem. Phys. **2**, 41 (1973); (c) L. Versluis and T. Ziegler, J. Chem. Phys. **322**, 88 (1988); (d) G. te Velde and E. J. Baerends, J. Comput. Phys. **99**, 84 (1992); (e) C. F. Guerra, J. G. Snijders, G. te Velde, and E. J. Baerends, Theor. Chem. Acc. **99**, 391 (1998).

[39] S. H. Vosko, L. Wilk, and M. Nusair, Can. J. Phys. **58**, 1200 (1980).
[40] A. D. Becke, Phys. Rev. A **38**, 3098 (1988).
[41] C. Lee, W. Yang, and R. G. Parr, Phys. Rev. B **37**, 785 (1988).
[42] D. J. Tannor and E. J. Heller, J. Chem. Phys. **77**, 202 (1982).
[43] M. E. Casida, C. Jamorski, K. C. Casida, and D. R. Salahub, J. Chem. Phys. **108**, 4439 (1998).
[44] E. J. Heller, R. L. Sundberg, and D. Tannor, J. Phys. Chem. **86**, 1822 (1982).